Interferometric Characterization of Keck Segment Edge Errors

Mitchell Troy,[a] Gary Chanan,[b] Mark Colavita[a] and Stephen J. Martinek[c]

[a]Jet Propulsion Laboratory, California Institute of Technology, Pasadena, CA 91109
[b]Department of Physics and Astronomy, University of California Irvine, Irvine, CA 92697
[c]4D Technology Corporation, Tucson, AZ 85706

ABSTRACT

The Keck telescope segments were manufactured by stressed mirror polishing of large circular pieces of Zerodur that were then cut into hexagons and finished by Ion Beam Figuring (IBF). It has long been believed that this process results in segments with little or no edge effects. As a result, this same general approach is planned for segment manufacturing for the Thirty Meter Telescope (TMT) and the European Extremely Large Telescope (E-ELT). However, recent measurements at the Keck telescope suggest that at least some of the Keck segments have significant aberrations within 60 mm of the edge. These aberrations impact the telescope phasing and the overall telescope image quality. We present interferometric measurements of multiple Keck segments, characterizing the surface errors near the edges over spatial periods from 5 cm down to 1 mm. We show that the largest phasing and image quality effects are due to plateaus of unremoved material, left behind after IBF as a result of obscuration by the IBF supports. Apart from these plateaus, the edge quality is relatively good, though not as good as in the segment interiors. Some residual phasing and image quality effects remain, and these are not currently understood.

Keywords: Telescopes, Segmented Mirrors, Optical Alignment, Phasing

1. INTRODUCTION

The Phasing Camera System (PCS)[1] is a Shack-Hartmann (SH) based phasing camera responsible for the optical alignment of the Keck telescopes. The segments of the telescopes are routinely phased to 30 nm Root Mean Square (RMS) surface piston error via the broadband (BB) phasing technique.[2] While this level of accuracy is currently sufficient for the Keck telescope, it is not sufficient for TMT. TMT has a requirement to phase the segments to better than 10 nm RMS surface. We have demonstrated that the narrowband (NB) phasing technique[3] can in principle achieve this accuracy. In fact this technique was originally developed for Keck, but subsequently abandoned in favor of the BB technique, which has a larger piston capture range and the advantage that it is not subject to aliasing effects.

As part of developing and demonstrating the required phasing accuracy for TMT, tests of NB phasing were conducted on the Keck telescopes. These tests revealed two effects. The first was phasing measurements that are wavelength dependent.[4] These chromatic errors are on the order of 25 nm (surface) over the wavelength span from 600 to 900 nm, as shown on the right panel of Figure 1. The left panel of Figure 1 illustrates the potential accuracy of NB phasing in the absence of chromatic effects, showing a residual of 4.9 nm square root of the sum of the squares (RSS), consistent with a measurement error of 10 nm for a single measurement.

The second effect observed from the NB phasing tests at Keck was a significant amount of diffracted light from some of the Keck segment edges. The BB and NB phasing techniques work by measuring the interference between two adjacent subapertures at the segment edges. This is accomplished by using a mask at the pupil plane of PCS that defines 120 mm diameter apertures (measured at the primary mirror (M1)) that are half on each segment edge. The left hand side of Figure 2 shows the phasing mask and associated subapertures. There are 84 intersegment edges; the inner 6 are obscured by the tertiary mirror support and another 6 are under the secondary mirror (M2) supports and therefore ignored in this analysis. There are also 35 subapertures along the

Further author information: Send correspondence to Mitchell Troy, mtroy@jpl.nasa.gov.

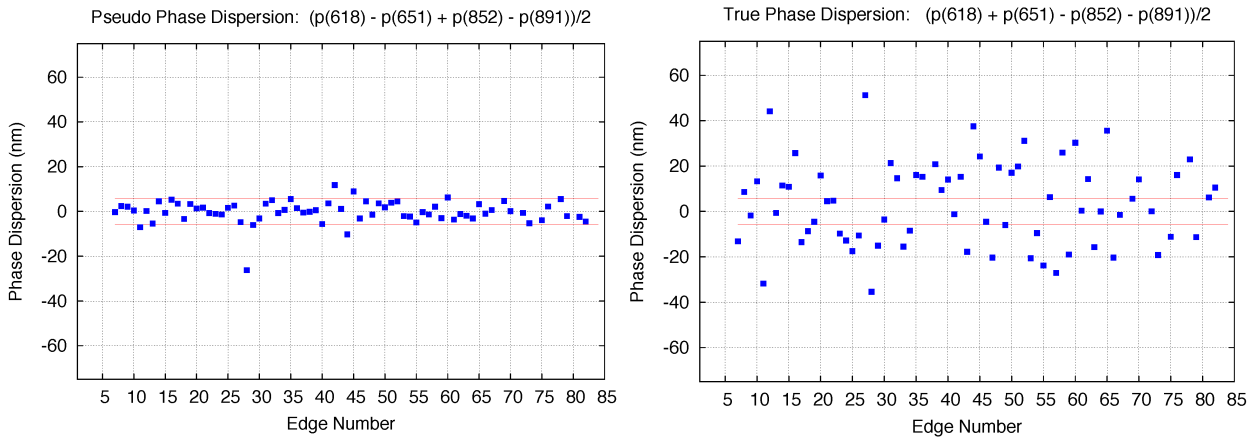

Figure 1. Two linearly independent linear combinations of phase measurements taken in four different filters. Left panel: The signs of the terms in the linear combination are chosen so that any wavelength dependence will approximately cancel out. Right panel: The signs are chosen so that any wavelength dependence will be enhanced. Horizontal lines represent the limits for random errors of the appropriate size. The larger scatter in the right plot is evidence of the systematic effect that we refer to as phase dispersion.

outer edge of the outer ring of segments. These subapertures are used to measure and register the re-imaged telescope pupil to phasing mask to a tolerance of better than 10 mm at M1.

Using the telescope Active Control System (ACS) it is possible to tilt segments out of the segment stack and still control the remaining segments. Using this technique we can measure the intensity of the semi-circular subapertures that lie only on a single segment. On the right hand side of Figure 2 Segment Position (SP) 8, 10, 12, 14, 16 and 18 are tilted out of the stack by ∼85 arcseconds. The two white circles (on SPs 6 and 15) indicate phasing subapertures that look as expected: elliptical images with approximately half the intensity of the full phasing subapertures. The two red circles highlight two subapertures (on SP 20 and 36) that have low intensity and form images that indicate significant wavefront error over the semicircle. About 25% of the 72 Keck segments have edges with a significant reduction ($> 20\%$) in intensity within $\pm$ 3.5 arcseconds.

These effects occur at both the center of the Keck segment edges (Location A in Figure 3) and when the phasing subapertures are shifted left or right by 200 mm on a segment edge (Locations B in Figure 3). However, both effects disappear when the subapertures are moved to the interior of a segment (Location C in Figure 3). Extensive analysis has been performed to attempt to explain the effects.[4–6] These effects do not arise from the algorithm, instrumentation, telescope, segment surface roughness, segment coatings or low spatial frequency errors over the phasing subapertures. The errors are largely tied to the segment surfaces themselves. That is, a given segment serial number (SN) edge is bad independent of which telescope and/or segment position it is installed in and the problem persists even if the segment is re-coated. This seems to leave only segment surface errors as the potential cause for the observed problems.

To confirm this prediction, we performed interferometric measurements of the surface error of 5 Keck segments. In Section 2 we describe the experimental setup, data collection procedure and summarize the data collected. In Section 3 we describe the data reduction steps and highlight some important problems uncovered. In Section 4 we describe our results and in Section 5 we summarize these results and discuss impacts of these errors on the future generation of giant segmented mirror telescopes (GSMTs).

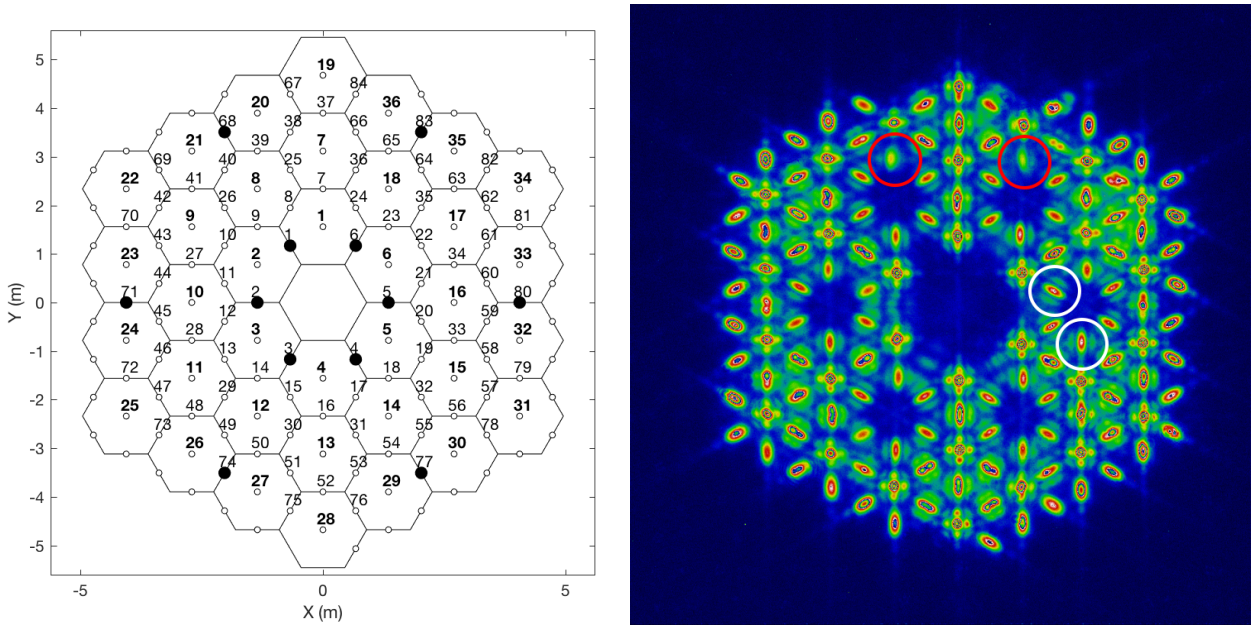

Figure 2. Left panel: the pupil mask used in PCS for phasing of the Keck telescopes. The intersegment subapertures are 120 mm in diameter (at M1). Right panel: phasing image taken with SPs 8, 10, 12, 14, 16 and 18 tilted out of the stack.

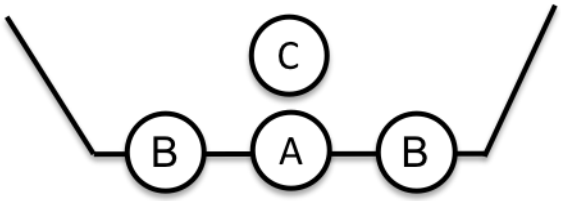

Figure 3. Locations where on-sky phase dispersion and scattered light data was collected from individual segments. See the text for further details.

2. EXPERIMENTAL SETUP AND PROCEDURE

The experimental setup used a 4D Technology AccuFiz H100S Fizeau Interferometer with a 6 Mega-Pixel detector, a 4" to 6" beam expander and a custom transmission sphere matched to the nominal 35 m Radius of Curvature (ROC) of the Keck segments, as shown in Figure 4. The individual phase measurements were made over a 6" diameter, in"dynamic mode", which uses a spatial carrier, with 32 frame averages. The dynamic mode collects all phase data in a single frame rather than over several frames and is highly insensitive to vibrations. The phase measurements had a sampling of 0.13 mm/pixel. The measurements at Keck also used an attenuation filter mounted between the transmission sphere and segment to balance test and reference beam intensity to obtain maximum fringe modulation.

Figure 5 shows the test setup at the Keck observatory. The interferometer is mounted on a custom handling cart. The interferometer platform is adjustable in height to select the measurement location on the segment, and in tip and tilt to null the tip/tilt fringes. The Keck segment being measured is shown mounted on its handling cart, which allows the segment to be rotated about the axis shown in the Figure.

The general data collection procedure was as follows:

1. Position the interferometer at X = 0, Y = 0, i.e., centered on the bottom horizontal edge of the segment.
2. Adjust the tip/tilt of the interferometer to null the fringes and collect a phase measurement.

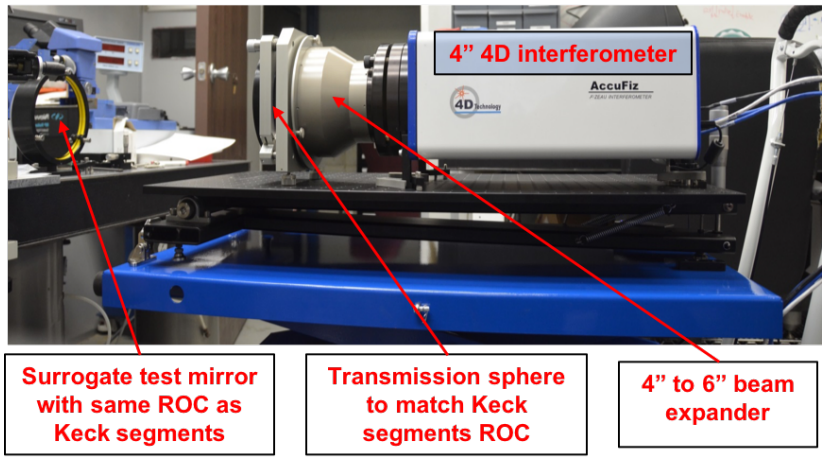

Figure 4. The interferometer and associated optics setup in the lab before shipment to the Keck summit.

Figure 5. The test setup at the Keck summit. The interferometer and associated optics are mounted on the blue handling cart. A Keck segment being measured is shown on its handling cart. The segment can be rotated to position any of the segment edges horizontal to the floor, allowing us to efficiently measure different locations on the segment without moving the interferometer. The attenuation filter mounted between the transmission sphere and segment to balance test and reference beam intensity to obtain maximum fringe modulation can also be seen in this figure.

3. Rotate the segment using its handling cart and measure the next segment edge at X = 0, Y = 0.
4. Repeat the above for all 6 segment edges.
5. Raise the height of the interferometer to the next Y location (still at X = 0) and collect data on all 6 edges.
6. After the desired Y heights are measured at X = 0, translate the interferometer to X = −200 mm, Y = 0 mm and repeat the above process.
7. Repeat the above for X = 200 mm.

The above procedure was efficient and we found we could make, record and store ≈ 25 measurements per

hour. Figure 6 shows the nominal measurement locations and Table 1 shows the segments measured and number of measurements per segment. A total of 336 unique locations were measured on 5 segments. The three high priority segments were selected because they had high on-sky phase dispersions and light loss. However, these three segments were also part way through the recoating process. The "washing" step resulted in streaks where the Al coating was partially removed. See Section 3.2 for details. Since we were initially not sure if we would be able to remove this effect, we measured two additional segments, S/N 88 and 51, that had not undergone this process.

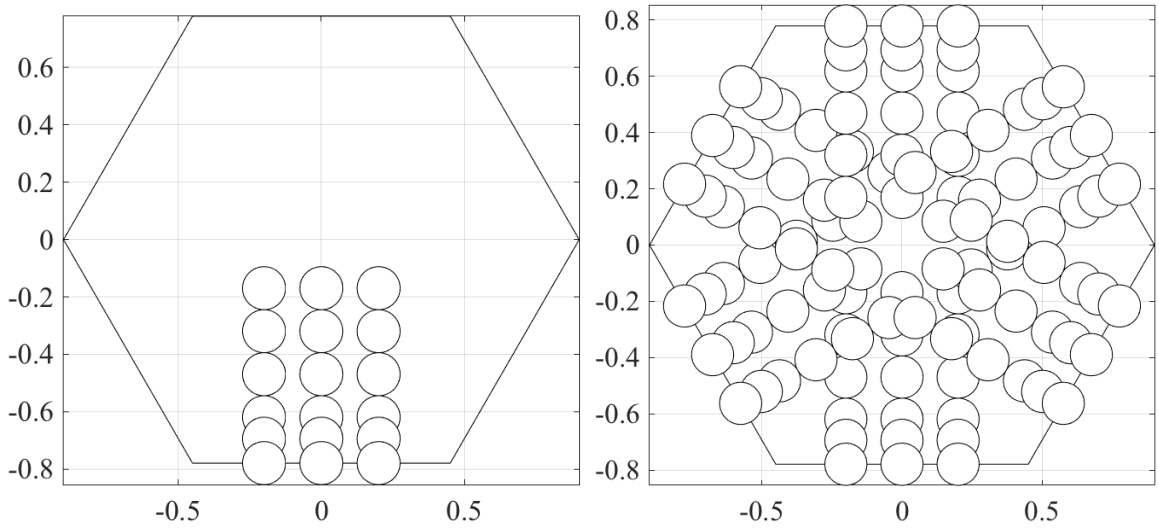

Figure 6. left panel: measurement locations for a single segment orientation. Right panel: measurement locations along all edges. The units on the X and Y axes are meters.

Table 1. Segments measured at Keck

Segment (S/N)	Number of Locations Measured	Comments
38	84	High priority
21	36	High priority
56	72	High priority
88	36	Freshly re-coated
51	108	Just removed from telescope
Total	336	

3. DATA REDUCTION

The input data for the data reduction process were the 32-frame averaged phase maps from the 4D interferometer. During the data calibration process the data were pre-processed to remove data drop outs, calibrated to correct for errors in the transmission sphere, and Zernikes 1-6 were removed to account for the design shape of the segments, as described in Section 3.1. As mentioned above several of the segments had artifacts from preparation for segment re-coating, and in section 3.2 we describe these effects and how they were removed from the data. In Section 3.3 we describe the observed IBF plateaus and the necessary steps to correctly account for these in the data reduction (Section 3.3). The data reduction software was written in Matlab, with the exception of the phase dispersion calculations, which employed the same Fortran algorithms used by PCS to insure consistency.

3.1 Data Calibration

The interferometer, beam expander and null lens all have wavefront errors that need to be subtracted from the measured phase maps. Calibration phase maps were generated each day we collected data for each segment.

The calibration phase maps were generated by averaging all data for a given segment for Y locations larger than 160 mm and smaller than 610 nm. This was to avoid any potential edge effects and the dimple in the center of the Keck segments. Once generated, the calibration maps were saved, and as part of the data processing the corresponding calibration map was subtracted from each phase measurement.

The above calibration corrects for any optical form errors in the null lens and the retrace error of the interferometer and beam expander as a result of the spatial carrier data acquisition technique. However, it does not correct for the nominal design shape of the Keck segments. In order to remove the design shape we remove Zernikes 1-6 (1st and 2nd order) from the phase measurements. The nominal design shape is dominated by segment local focus, astigmatism and some coma which will appear as 1st and 2nd order Zernikes over the 6" measurement diameter. This procedure worked well, but is not ideal. In the future we hope to look at removing the actual design shape for each measurement location.

3.2 Effects from Segment Re-Coating Preparation

Three of the segments we measured (SN 36, 72 and 84) had undergone the first step of the re-coating process which consists of washing with a chemical agent. This resulted in streaks in the phase maps corresponding to where the Al coating was partially removed. The observed streaks were parallel to edge between vertices 1 and 6, which is consistent with how the mirrors were washed. This was further proved by re-washing a small portion of the segment and making interferometric measurements before and afterwards. This error looks similar to the effect we were expecting to see, but is unrelated.

Using a Fourier filter we were able to effectively remove the artifacts by filtering out spatial frequencies within $\pm$ 25 deg. of the washing direction. Figure 7 shows an example phase map before and after application of the Fourier filter. However, this process does artificially reduce the RMS surface error. To quantify the magnitude of the reduction, this process was also run on the data from the two segments that had not been prepared for re-coating and did not have the washing artifacts. These data showed a 17% reduction in the RMS surface after filtering. Thus, all data presented here for which the filtering was applied have their RMS values increased by the 17% to account for this effect.

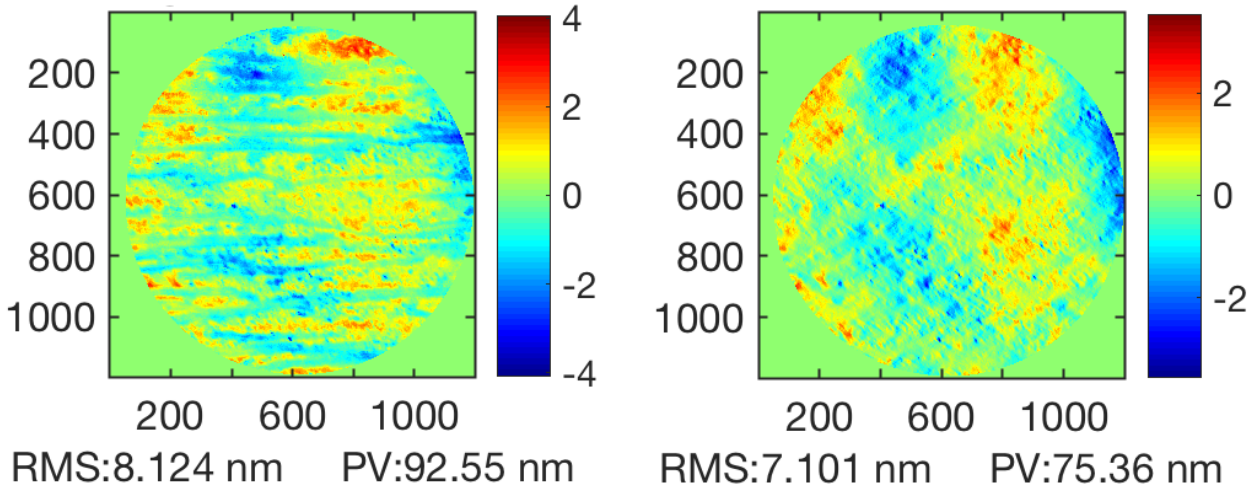

Figure 7. Left panel: an example (SN 38, Edge 56 X = 0,Y = 610 mm) of a phase measurement of a segment that has undergone the first step of the re-coating process. Right panel: the resulting image after Fourier filtering to remove the effect. The horizontal artifacts are removed. See the text for more details.

3.3 IBF Plateaus

During IBF the segments were supported underneath by "J-Hooks", as shown in Figure 8. As a result the area under these supports was not exposed to the IBF beam and in at least some cases plateaus were left behind. The left hand side of Figure 9 shows an example of a measured plateau at X = 0. These plateaus are approximately

60 mm by 30 mm and have heights from 200-800 nm. The central image of Figure 9 shows an interferometer measurement made at X = 200, which contained the surprising result of an IBF plateau. In the past we have argued[5] that the measurements at X=± 200 demonstrate that there is significant variation of subimage intensity and phase dispersion along a segment edge and so the effects at X = 0 could not be explained by IBF plateaus. This has turned out to be incorrect as there are in fact plateaus located in some of the X = ± 200 data. It appears that after the first 3 segments (SN: 09, 35 and 38) had undergone IBF, the J-Hooks were moved to the other 3 segment edges, and changed from a single support at X=0 to be two supports located at X=± 275 mm; each J-Hook still appears to obscure an area 60 by 30 mm. .

The right panel of Figure 10 shows the phasing mask, which masks out 30 mm parallel to the segment edges, and includes a vertical mask (for symmetry) also 30 mm wide. Example phase measurements at X = 0 and X = 200 are shown in this Figure with the phasing mask applied. In the X=0 case the plateaus account for 25% of the phasing subaperture area. As a result it should not be a surprise that they introduce phase dispersion and scattered light. On-sky measurements at X = ± 200 mm were also impacted by the previously unknown IBF plateaus at X = ± 275 mm.

Any IBF plateaus are excluded from the calculations during the Zernike removal (Section 3.1) and removal of effects from segment re-coating (Section 3.2) steps to avoid biasing the results. After these steps we generated the final phase maps both with and without the IBF plateaus included in the various calculations.

Figure 8. A Keck segment in the IBF chamber. The first three segments were supported at the centers of three of the segment edges.

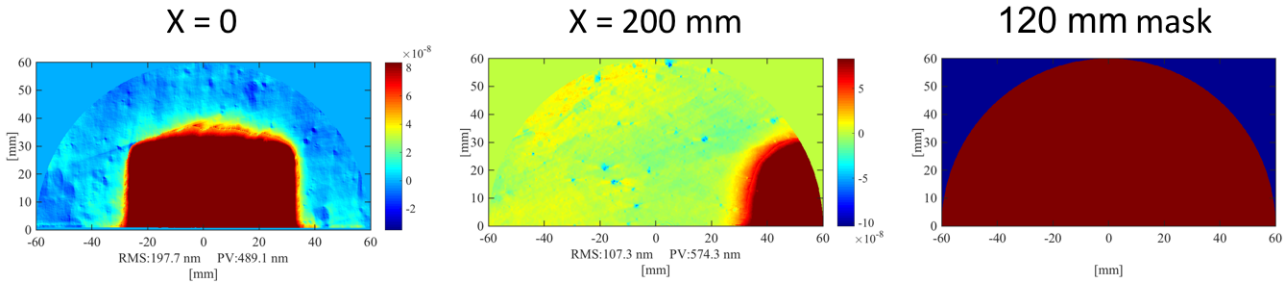

Figure 9. Left panel: an example of a phase measurement at X = 0, Y = 0 and an IBF plateau at X = 0. Central panel: a phase measurement at X = 200 and one of the IBF plateaus located at X = 275 mm. Right panel: the mask that was applied to this data, shown as reference.

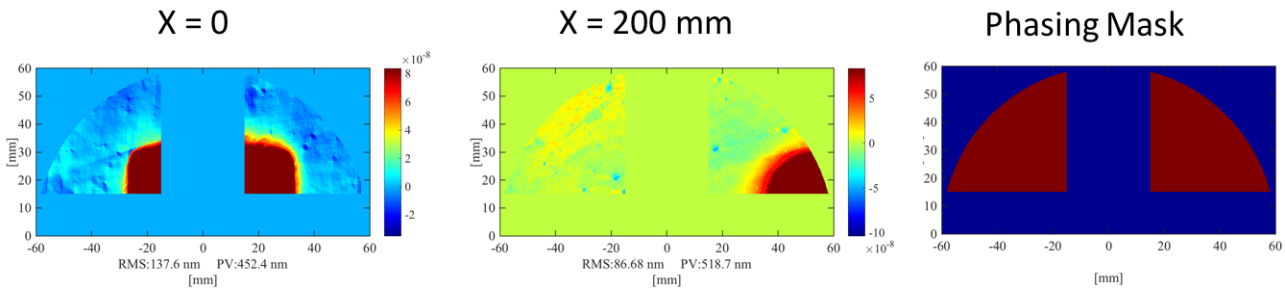

Figure 10. The right panel shows the PCS phasing mask which blocks light in a 30 mm horizontal strip (to block the segment gap) and for symmetry blocks a vertical 30 mm wide strip. In the left and center panels the phasing mask has been applied to the X=0 and X=200 phase measurements shown in Figure 9.

4. RESULTS

In the following sections we describe the three metrics we have used to evaluate the segment quality: RMS surface error, fractional intensity (or scattered light) and phase dispersion.

4.1 RMS Surface Error

The calculated RMS surface error for each measurement is shown in Figure 11 after application of the data reduction discussed in Section 3; the markers are centered on the measurement location, but the diameters are half that of the true diameter, to avoid overlapping in the plot. It can be seen that when measurements were made at the locations of the IBF plateaus, these dominate the RMS surface error. SN 38 had the IBF supports in the initial locations (centered on the segment edges) and the remaining measured segments had them located on the opposite 3 edges and at $X = \pm$ 275 mm. Figure 12 shows the RMS surface error when the 60 x 30 mm plateaus are excluded from the RMS surface error calculation. There appears to be a general increase in RMS surface error toward the outer edge of the segment. In Figure 13 the mean RMS surface error as a function of distance from the segment edge is plotted for each segment. There is an increase in the RMS surface error which starts to occur at $\approx$ 200 mm from the edge of the segment. This is not currently understood, as this is relatively far from the edge of the segment and IBF should be able to polish the segment all the way out to the edge. SN 88, which is the best segment, does not show this effect so it appears the cause may not be a fundamental limitation of IBF. The TMT requirement for spatial periods between 8 and 50 mm is 5 nm RMS surface. This spatial period corresponds well to these measurements. The Keck segments did meet the Keck specifications and they are close to (or in some cases meet) the TMT specifications. This seems to indicate that the basic process of Stress Mirror Polishing (SMP) of circular roundels, hex cutting them and then performing IBF can meet the TMT specification.

4.2 Measurement Noise

We calculated the random measurement noise by taking quality control measurements using the 4D's 4Sight data acquisition and analysis software. In this mode the software took five data sets of 32 frame averages. We then calculated the RMS over the five data sets for each pixel and calculated the median value of all the RMS values. A total of nine quality control measurements were taken over the four days; the mean measurement noise was 1.4 nm, the minimum was 0.93 nm, and the maximum was 2.0 nm (RMS surface).

We also calculated the measurement repeatability; that is, how repeatable is a measurement after both the segment and interferometer are moved and re-aligned. A total of 3 repeatability tests were executed on different days with typically four or more hours between the measurements. In this case we subtracted the two calibrated phase maps and calculated the RMS of the difference and divided by $\sqrt{2}$ to get the repeatability of a single measurement. The mean measurement repeatability was 1.8 nm, the minimum was 1.2 nm, and the maximum was 2.6 nm (RMS surface).

The measurement noise and repeatability are significantly smaller than the segment phase errors and should not be contributing significantly to the RMS values we report in this paper.

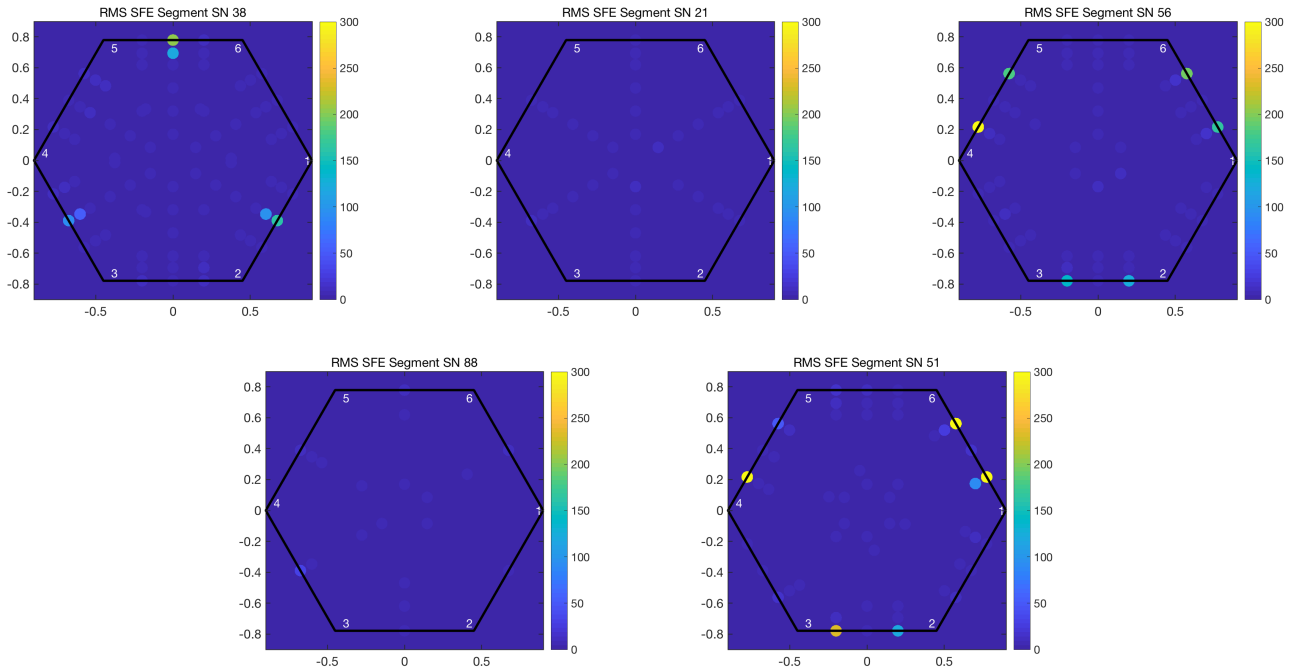

Figure 11. RMS surface error (nm) for each measurement made on the segments. For those segments (SN 38, 56, 51) which included measurements of at the locations of the IBF plateaus. The plateaus dominate the RMS. Note that the center of the circles indicate where the measurements were made, but their diameter is half that of the actual diameter.

4.3 Predicted Fractional Intensity

Given a measured phase map we can predict the edge intensity from the half-illuminated segment edges as they would be measured them on-sky. If the edge is not at Y = 0 then we split the full 150 mm diameter map into two, as if the top half and bottom half correspond to phase measurements from the segment edges. Then the phasing mask (Section 3.3) is applied, the Point Spread Function (PSF) calculated at the appropriate wavelength (852 nm) and the fractional light in a box 7.0 arcseconds on a side is calculated. The exact registration of both the on-sky and interferometer data with respect to the segment is not known; to estimate the uncertainty in the predicted fractional light the registration of the phasing mask to the segment is varied by ± 10 mm in X and Y and the above calculation repeated.

The left panel of Figure 14 compares the on-sky and predicted edge intensity for the locations where we have both measurements. There are 4 cases that included IBF plateaus, and for those cases there is good agreement between the on-sky and predicted fractional light. It is clear that IBF plateaus can and do scatter large amounts of light. When there are no plateaus the interferometer measurements predict almost no scattered light and that matches a majority, but not all of, the on-sky data. On the right panel of Figure 14 the edge intensity is plotted for all of the on-sky data as a function of segment SN. Green markers indicate measurement locations where there were no IBF supports and black markers those locations that did contain these supports. Again, it is clear that IBF plateaus can scatter large amounts of light; however, there are also a few cases of significant scattered light where no plateaus should exist.

4.4 Predicted Phase Dispersion

Given a measured phase map we can also predict the phase dispersion from the half-illuminated segment edges as they would be measured on-sky. If the edge is not at Y = 0 then we split the full 150 mm diameter map into two, as if the top half and bottom half correspond to phase measurements from the segment edges. Then the phasing mask (Section 3.3) is applied and the PSFs calculated at the appropriate wavelengths (651 and 852 nm). The PCS phasing algorithm is then run on both PSFs, and the phase dispersion is calculated. The exact registration

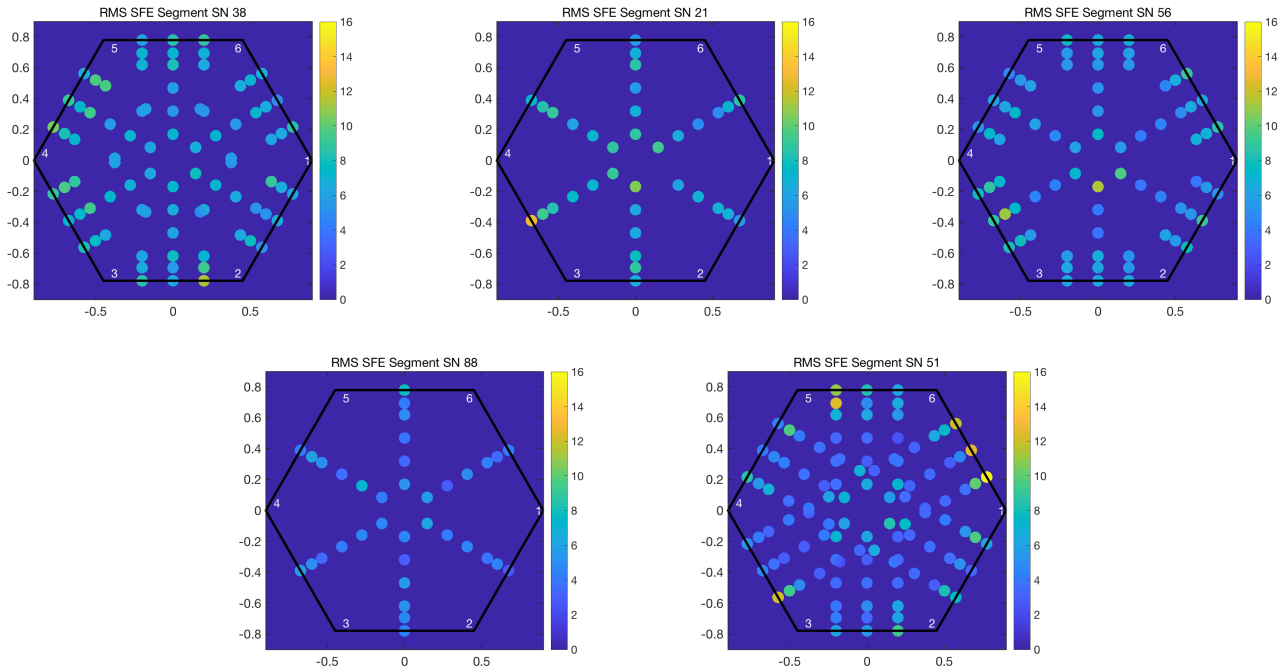

Figure 12. RMS surface error (nm) for each measurement made on the segments. However, unlike Figure 11 in this Figure the 60 by 30 mm IBF plateaus were excluded from the RMS calculation. Note that the circles indicate where the measurements were made, but their diameter is half that of the actual measurement diameter.

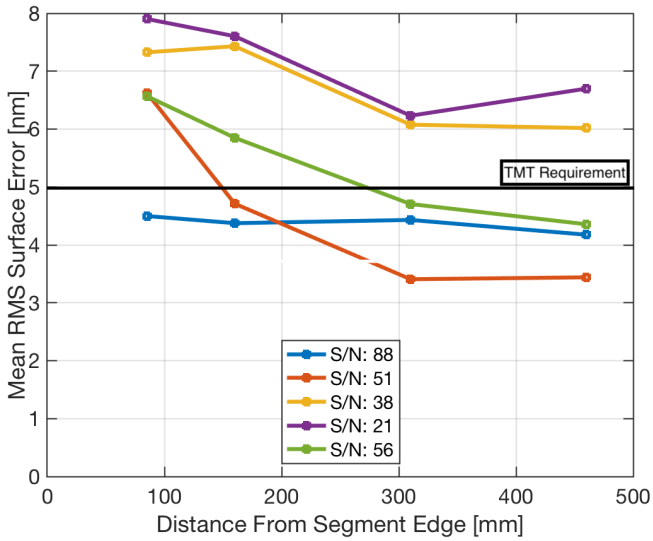

Figure 13. Mean RMS surface error as a function of distance from the segment edge for each measured segment. There is in general a trend that the RMS surface error starts to increase towards the edge of the segment starting at $\approx$ 200 mm from the segment edge. See the text for a description of the TMT requirement.

of both the on-sky and interferometer data with respect to the segment is not known; to estimate the uncertainty in the phase dispersion the registration of the phasing mask to the segment is varied by $\pm$ 10 mm in X and Y and the above calculations repeated.

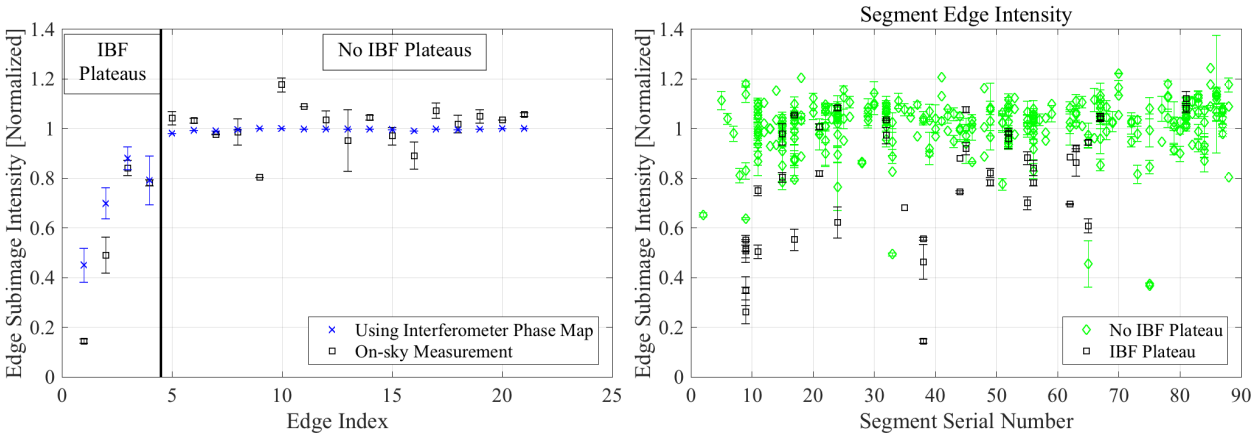

Figure 14. Left panel: a comparison of the on-sky and predicted fractional intensity. Right panel: on-sky fractional intensity with green indicating locations on the segment where there were no IBF supports and black indicating locations that had them. See the text for a detailed description of both plots.

The left panel of Figure 15 compares the on-sky and predicted phase dispersion for the locations where we have both measurements. For the two cases that included IBF plateaus, there is reasonably good agreement between the on-sky and predicted results. It is clear that IBF plateaus can and often do cause significant phase dispersion. When there are no plateaus the interferometer measurements predict almost no phase dispersion. However, we still observe on-sky phase dispersion in these cases. On the right panel of Figure 15 the histogram of all ≈ 600 measurements is shown. The edges without IBF plateaus have a very tight distribution with the largest value being 3 nm. However, the edges with plateaus have a distribution with a much larger tail and errors; $\approx 33\%$ of the data has values larger than 3 nm.

Figure 16 shows the on-sky measured phase dispersion with the IBF plateau data shown in blue crosses. The RMS of this data is 53 nm while that of the data without plateaus is 17.7 nm. Clearly the on-sky phase dispersion is dominated by the plateaus, but they are not the only cause of phase dispersion. This remaining phase dispersion is larger than can be accounted for by the 5 nm measurement noise of phase dispersion.

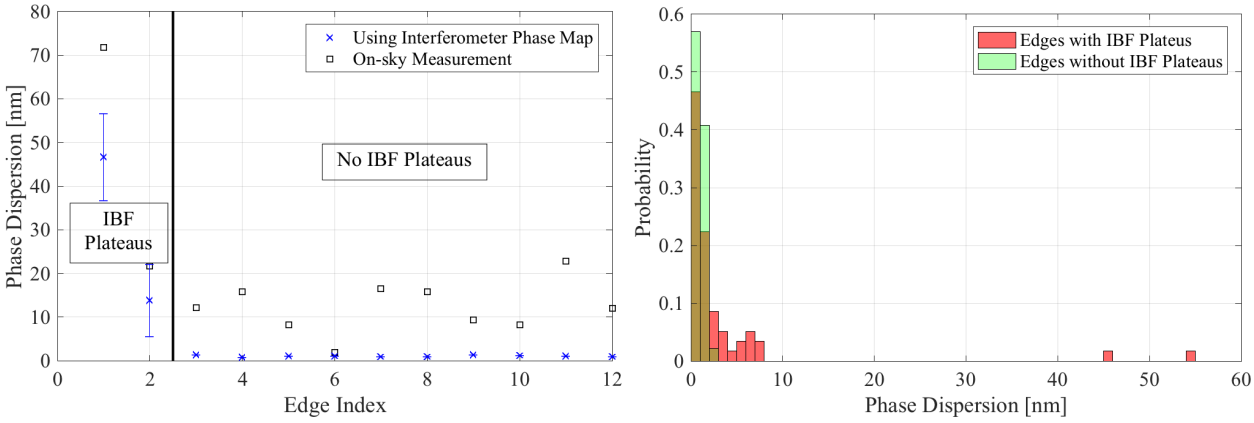

Figure 15. The left panel shows a comparison of the on-sky and predicted phase dispersion. The right panel shows the histogram of all predicted phase dispersion calculated from the interferometer phase maps. See the text for a detailed description of both plots.

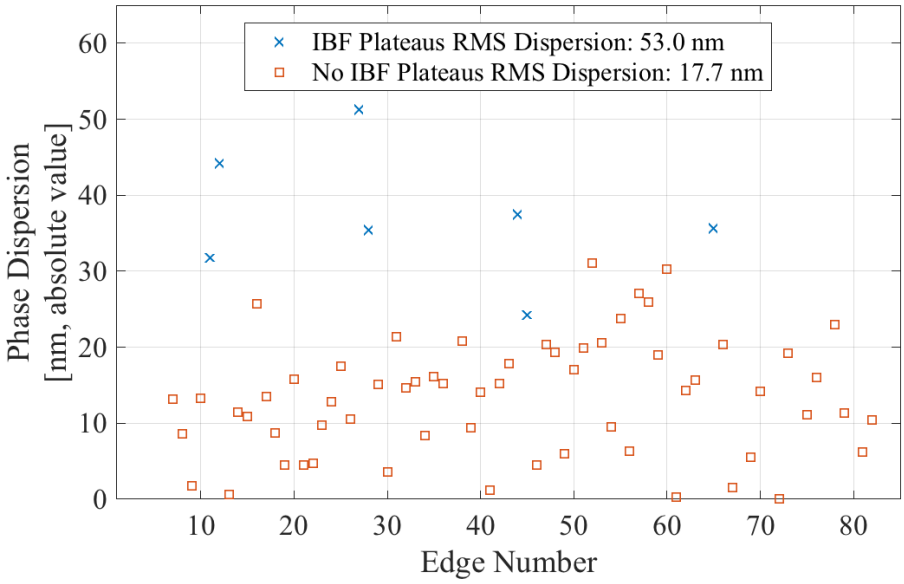

Figure 16. The measured on-sky phase dispersion shown for Keck II. The blue crosses indicate data where IBF supports were located at the phasing subaperture locations.

5. CONCLUSIONS

In summary, the largest phase dispersion and scattered light errors from the Keck segments are caused by IBF plateaus. These plateaus have caused significant confusion as the precise location of plateaus at X = ± 275 mm was unknown until these measurements were made. On-sky data collected at X = ± 200 mm in an effort to rule out IBF plateaus as a cause of these errors was impacted by these plateaus. In addition the spatial extent of plateaus at X=0 are also larger than previously understood. While IBF of optics is typically done with supports at the periphery of the optical surface, this work demonstrates that for GSMTs or any optics where the clear aperture needs to match the full aperture the optic should be supported from behind to avoid creation of IBF plateaus.

These measurements have helped to understand phasing and related issues at Keck and in the process reduce risk for TMT. The Keck segment RMS surface measurements have demonstrated that meeting the TMT 5 nm RMS surface specifications for spatial periods between 8 and 50 mm is achievable. There is an increase in RMS surface error starting at ≈ 0.2 meters from the edge of the segment that we did not expect and can not currently explain.

The on-sky Alignment and Phasing System (APS) measurements show residual phase dispersion of ≈ 18 nm that is not attributable to IBF plateaus that is not currently understood. There is some indication that on Keck 2 a portion of this error could be related to a mis-registration in rotation between the PCS and the telescope pupil.[6] We plan to correct the rotational error, re-measure the phase dispersion and continue to look for the cause of any remaining phase dispersion. Reducing this phase dispersion by a factor of 2 to 3 is not required for Keck, but is required for TMT, which needs the narrowband phasing approach[3] both to meet the required increase in phasing accuracy (30 vs 10 nm RMS surface) and in measurement speed (up to five times faster).

ACKNOWLEDGMENTS

This research was carried out in part at the Jet Propulsion Laboratory, California Institute of Technology, under a contract with the National Aeronautics and Space Administration.

The authors gratefully acknowledge the support of the TMT collaborating institutions. They are the California Institute of Technology, the University of California, the National Astronomical Observatory of Japan, the National Astronomical Observatories of China and their consortium partners, the Department of Science and Technology of India and their supported institutes, and the National Research Council of Canada. This work was supported as well by the Gordon and Betty Moore Foundation, the Canada Foundation for Innovation, the Ontario Ministry of Research and Innovation, the Natural Sciences and Engineering Research Council of Canada, the British Columbia Knowledge Development Fund, the Association of Canadian Universities for Research in Astronomy (ACURA), the Association of Universities for Research in Astronomy (AURA), the U.S. National Science Foundation, the National Institutes of Natural Sciences of Japan, and the Department of Atomic Energy of India.

We would like to thank the W. M. Keck Observatory for their support of these measurements.

REFERENCES

1. Chanan, G., Nelson, J., Mast, T., Wizinowich, P. L., and Schaefer, B. A., "W.M. Keck Telescope phasing camera system," *Proc. SPIE* **2198**, 1139–1150 (June 1994).
2. Chanan, G., Troy, M., Dekens, F. G., Michaels, S., Nelson, J., Mast, T., and Kirkman, D., "Phasing the mirror segments of the Keck telescopes: the broadband phasing algorithm," *Applied Optics* **37**, 140–155 (Jan. 1998).
3. Chanan, G., Ohara, C., and Troy, M., "Phasing the mirror segments of the Keck telescopes: the narrowband phasing algorithm," *Applied Optics* **39**, 4706–4714 (Sep. 2000).
4. Chanan, G., Troy, M., and Raouf, N., "Phasing the segments of the Keck and Thirty Meter Telescopes via the narrowband phasing algorithm: chromatic effects," *Proc. SPIE* **9906**, 1184–1191 (Jul. 2016).
5. Troy, M., Chanan, G., and Brock, N., "Keck segment surface artifacts: Impacts on segment phasing and image quality," in [*Proceedings of the Adaptive Optics for Extremely Large Telescopes 5*], Instituto de Astrofsica de Canarias (2017).
6. Chanan, G. and Troy, M., "Chromatic effects in narrowband phasing of the Keck telescope segments: Theory and numerical simulations," *Proc. SPIE* **this volume** (Jun. 2018).